European Journal of Mechanics / A Solids 85 (2021) 104081

Contents lists available at ScienceDirect

European Journal of Mechanics / A Solids

journal homepage: http://www.elsevier.com/locate/ejmsol

The contribution of mechanical interactions to the constitutive modeling of fiber-reinforced elastomers

M.R. Mansouri [a,*], P.F. Fuchs [a], J.C. Criscione [b], B. Schrittesser [a], J. Beter [a]

[a] Polymer Competence Center Leoben GmbH, 8700, Roseggerstreet 12, Leoben, Austria
[b] Department of Biomedical Engineering, Texas A&M University, College Station, TX, 77843-3120, College Station, USA

ARTICLE INFO

Keywords:
Mechanical interaction potential
Constitutive behavior
Fiber-reinforced elastomers
Non-symmetric deformations
Composite laminates

ABSTRACT

Hyperelastic fiber-reinforced materials are conventionally modeled based on the contributions of their constituent materials. A unified invariant-base constitutive model, named Matrix-Fiber-Interaction (MFI) model, is proposed to take into account particularly the mechanical interaction contribution of the constituent materials in fiber-reinforced elastomers with two fiber families. Its high predictive capability for the modeling of the behavior of composites with different material anisotropy is verified by several experiments. This model along with its structurally based framework of material characterization allows measuring distinct contributions of the matrix, fiber, and mechanical interactions in the sense that the latter can be determined regardless of the functional form of the fiber potential. Therefore, in this paper, the MFI model implemented in a user-defined subroutine is used to highlight the importance of mechanical interaction potential. Using three representative examples: uniaxial extension of single-layer plates with different material anisotropy, inflation-extension of a thin cylindrical tube, and load-coupling behaviors in composite laminates, its effect is analyzed. The comparisons of experiments with simulation results underline the prediction quality improvement using the interaction potential in the modeling of single-layer composites. For the two latter deformations, the simulation results comparatively indicate the effect of mechanical interaction potential for the modeling of more complicated structures.

1. Introduction

Flexible fiber-reinforced materials, including biological organs and inorganic composites, are considered as hyperelastic continuums in the sense that it is assumed there exists a potential function Ψ which represents the total stored energy of the continuum during the deformation. The majority of the works in the field of flexible fiber-reinforced materials are taken into account the potentials of the individual constituent materials, i.e. soft matrix and fibers, to model their constitutive behaviors. The papers by, for example, Holzapfel and Gasser (2001), Milani and Nemes (2004), Merodio and Saccomandi (2006), Ren et al. (2011), Fereidoonnezhad et al. (2013), Chebbi et al. (2016), Liu et al. (2019), Connolly et al. (2019) accounted the contributions of the matrix and fibers as constituent materials for modeling inorganic fiber-reinforced composites. In addition to, the works by Holzapfel et al. (2000), Murphy (2013), Alhayani et al. (2014), Tricerri et al. (2016), Chaimoon and Chindaprasirt (2019) are examples in which the contributions of the constituent materials are only considered for mechanical behavior modeling of soft biological tissues. Among others, Holzapfel-Gosser-Ogden (HGO) model (Holzapfel et al., 2000) provides a nice comparison between various relations for fibrous biological tissues. This model is also used frequently for constitutive modeling of the inorganic materials. We make no attempt to list a large number of the works done in this subject.

A few works considered the mechanical interaction potential for constitutive modeling of flexible fiber-reinforced materials. The interaction potential is introduced for the first time by Wagner and Lotz (2004) and Peng et al. (2006) for modeling the mechanical behavior of human annulus fibrosus. Since then, the interaction potential appears to be taken into account for modeling of cord-rubber composite (Peng et al., 2013), biological tissues (Guo et al., 2006), soft inorganic composites (Gong et al., 2016), and dry fabrics (Gong et al., 2017). Recently, Melnik et al. (2018) and Holzapfel and Ogden (2019) considered an interaction potential associated with coupling between dispersed collagens and cross-links for modeling of soft tissues. However, very little is known about the efficacy of including interaction potential in the constitutive behavior modeling of flexible fiber-reinforced materials.

The main goal of the present study is to propose a unified invariant-

* Corresponding author.
E-mail address: mohammad.mansouri@pccl.at (M.R. Mansouri).

https://doi.org/10.1016/j.euromechsol.2020.104081
Received 21 February 2020; Received in revised form 6 July 2020; Accepted 11 July 2020
Available online 6 August 2020

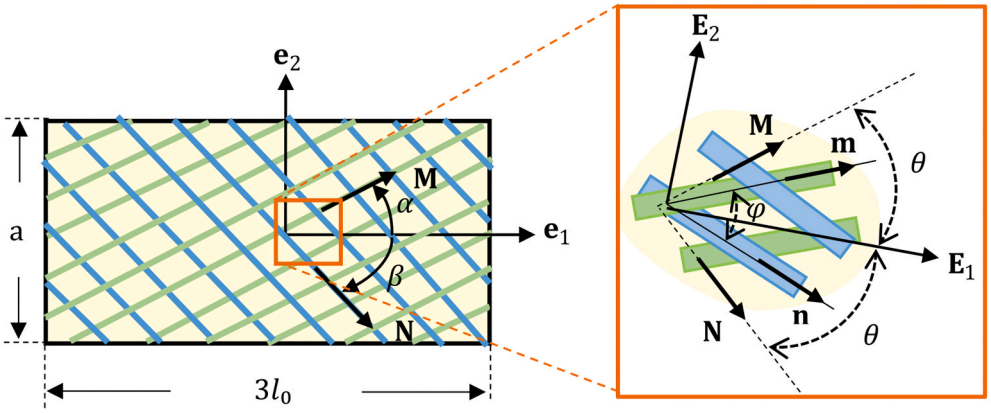

Fig. 1. Model geometry of the composite strips, left, with two fiber families $\boldsymbol{M} = \cos\theta\,\boldsymbol{E}_1 + \sin\theta\,\boldsymbol{E}_2$ and $\boldsymbol{N} = \cos\theta\,\boldsymbol{E}_1 - \sin\theta\,\boldsymbol{E}_2$, which are initially located in the reference configuration, right. The θ is half of the angle subtended by $\boldsymbol{M}$ and $\boldsymbol{N}$. Under a uniaxial extension in the loading direction $\boldsymbol{e}_1$, they are mapped to the spatial line elements $\boldsymbol{m}$ and $\boldsymbol{n}$ in the final configuration with the angle ϕ between. For simplicity, a fixed coordinate system $\{\boldsymbol{e}_1, \boldsymbol{e}_2, \boldsymbol{e}_3\}$ is here adopted for specifying the loading direction.

base constitutive model, so-called the MFI model, on the basis of extensional- and angular-base deformation invariants to take into account particularly the contribution of the mechanical interactions between constituent materials of the fiber-reinforced elastomers with two fiber families. It introduces a structurally based framework for characterizing the mechanical interactions regardless of the functional form of the fiber potential. Therefore, during a specific deformation, the contribution of mechanical interactions can be obtained without being perturbed by other contributions. Moreover, we take advantage of this model and capabilities of existing commercial software for nonlinear analysis in order to highlight for the first time the importance of the mechanical interaction potential in constitutive modeling of fiber-reinforced elastomers.

2. Model description

2.1. Kinematics

In this section, the notation and fundamental concepts of nonlinear continuum mechanics are outlined in order to describe the MFI constitutive model, the elasticity tensors and corresponding Cauchy stresses. Consider a continuum body B_r in the reference configuration of a material body. It is supposed that any material point be labelled by its position vector $\mathbf{X}$ in B_r. Let the body be deformed into the new configuration B so that the material point $\mathbf{X}$ takes up the position $\mathbf{x}$. This motion is introduced by the mapping $\mathbf{x} = \chi(\mathbf{X})$. The gradient of χ is defined by $\mathbf{F}(\mathbf{X}) = \mathrm{Grad}\ \mathbf{x}$ and referred to as the deformation gradient tensor that its determinant $J = \det\mathbf{F}(\mathbf{X}) > 0$ is called the local volume ratio. In terms of $\mathbf{F}$ the right Cauchy-Green strain tensor is given by $\mathbf{C} = \mathbf{F}^{\mathrm{T}}\mathbf{F}$ with the corresponding first and second invariants as

$$I_1 = \mathrm{tr}\,\mathbf{C} \quad \text{and} \quad I_2 = \frac{1}{2}\left[(\mathrm{tr}\mathbf{C})^2 - \mathrm{tr}\left(\mathbf{C}^2\right)\right] \tag{1}$$

Consider two material line elements in a fiber-reinforced material initially aligned along the unit vectors defined as $\mathbf{M} = \cos\theta\,\mathbf{E}_1 + \sin\theta\,\mathbf{E}_2$ and $\mathbf{N} = \cos\theta\,\mathbf{E}_1 - \sin\theta\,\mathbf{E}_2$, which are initially located in reference configuration, as shown in the right-hand side of Fig. 1. The parameter θ is half of the angle subtended by $\mathbf{M}$ and $\mathbf{N}$. They are mapped to the spatial line elements $\mathbf{m}$ and $\mathbf{n}$ in the final configuration by deformation gradient $\mathbf{F}$ through the motion $\mathbf{x} = \chi(\mathbf{X})$. During this deformation, the material line elements might experience a change of both the element length and the angle. Spencer (1984) introduced the pseudo-invariants for fiber-reinforced materials as follows,

$$I_4(\mathbf{M}) = \mathbf{C} : \mathbf{M} \otimes \mathbf{M}, \quad I_6(\mathbf{N}) = \mathbf{C} : \mathbf{N} \otimes \mathbf{N}, \quad I_8(\mathbf{M}, \mathbf{N}) = \mathbf{C} : \mathbf{M} \otimes \mathbf{N} \tag{2}$$

The pseudo-invariants I_4 and I_6 capture information about the square of stretch in the fiber directions $\mathbf{M}$ and $\mathbf{N}$, respectively. In the original work of Criscione and Hunter (2003), they introduced a scalar $\mathscr{B}$ that represents a change of the angle between equally deformed fibers. They found a relation between $\mathscr{B}$, the angle between deformed fibers (denoted by ϕ), and the right-hand side of the relations in (2) as

$$\cos\phi = \frac{\mathbf{C} : \mathbf{M} \otimes \mathbf{N}}{\sqrt{\mathbf{C} : \mathbf{M} \otimes \mathbf{M}}\sqrt{\mathbf{C} : \mathbf{N} \otimes \mathbf{N}}} = \frac{\mathscr{B}^2\cos^2\theta - \mathscr{B}^{-2}\sin^2\theta}{\mathscr{B}^2\cos^2\theta + \mathscr{B}^{-2}\sin^2\theta} \tag{3}$$

Upon replacing the relations (2) in (3), an angular-base invariant set in terms of the strain invariants as $I_8^* = I_8/\sqrt{I_4\ I_6} = \cos\phi$ is considered here to take into account the current angle between deformed fibers.

2.2. Modeling the mechanical interactions of the constituent materials

The extensional-base invariants I_4 and I_6 as well as the angular-base invariant I_8^* are employed by the fibers and mechanical interaction potentials, respectively, to form the MFI constitutive model (after the first initials of the contributions' names, i.e. Matrix-Fiber-Interaction) as

$$\Psi(\mathbf{C}, \{\mathbf{M}, \mathbf{N}\}) = \Psi_{\mathrm{M}}(I_1) + \Psi_{\mathrm{F}}(I_4, I_6) + \Psi_{\tau}\left(I_8^*\right) - \frac{1}{2}q(I_4 - 1) - \frac{1}{2}r(I_6 - 1)$$
$$\begin{cases} I.\ \text{inextensible fibers} & I_4, I_6 = 1 \\ II.\ \text{extensible fibers} & q, r = 0 \end{cases} \tag{4}$$

with the respective deformation gradient

$$\mathbf{F} = \mathbf{Q}\,\mathbf{f} \tag{5}$$

where $\mathbf{Q}$ is a proper orthogonal tensor such that $\mathbf{Q}^{\mathrm{T}}\mathbf{Q} = \mathbf{I}$ and $\det\mathbf{Q} = 1$. The scalar quantities q and r are fiber tensions as reactions associated with the inextensibility constraints $I_4 = 1$ and $I_6 = 1$, respectively. Adding the term $\frac{1}{2}q(I_4 - 1) + \frac{1}{2}r(I_6 - 1)$ in Eq. (4) is relied on the fact that the mechanical interaction potential is a result of the rotation of fibers and not of the fibers' elongation. This term provides a structurally based framework for characterization of the mechanical interaction properties so as to enable them to be found regardless of the functional form of fibers potential. This experimental framework will be further elaborated in upcoming works. It is emphasized that since the fibers are generally

assumed to be extensible, this term is not considered for the computational implementation of the model, i.e.

For an incompressible and thin composite, it is straightforward to find specific forms of the deformation gradients associated with the constraints I and II, defined in Eq. (4), as $\mathbf{F}_I = \mathbf{Q}\,\mathbf{f}_\phi^*$ and $\mathbf{F}_{II} = \mathbf{Q}\,\mathbf{f}_\mathrm{f}^*$, respectively (it is shown in detail in Appendix A). f_ϕ^* represents specifically change of the angle between fibers while $\mathbf{f}_\mathrm{f}^*$ accounts the elongation of the fibers. Accordingly, the constitutive model in Eq. (4) is specialized as

$$\Psi_I = \Psi_\mathrm{M}(I_1,\ I_2) + \Psi_\tau(I_8^*) - \frac{1}{2}q(I_4-1) - \frac{1}{2}r(I_6-1), \qquad \mathbf{F}_I = \mathbf{Q}\,f_\phi^* \tag{6}$$

$$\Psi_{II} = \Psi_\mathrm{M}(I_1,\ I_2) + \Psi_\mathrm{F}(I_4,\ I_6), \qquad \mathbf{F}_{II} = \mathbf{Q}\,\mathbf{f}_\mathrm{f}^* \tag{7}$$

The relations (6) and (7) introduce a new framework for material characterization of the mechanical interaction properties and fibers, respectively, which will be discussed in detail in upcoming works.

2.3. Energy functions

In a fiber-reinforced elastomer, as mentioned by Holzapfel and Ogden (2009), it is convenient and customary to make no distinction between the directions $\mathbf{M}$ and $-\mathbf{M}$ ($\mathbf{N}$ and $-\mathbf{N}$). Since $\Psi_\mathrm{F} = \Psi_\mathrm{F}(\mathbf{C}, \mathbf{M}\otimes\mathbf{M},\ \mathbf{N}\otimes\mathbf{N})$, the fiber potential is an even function while $\Psi_\tau = \Psi_\tau(\mathbf{C}, \mathbf{M}\otimes\mathbf{N})$ is an odd function. Therefore, the interaction potential Ψ_τ can depend on the sign of arbitrary directions. To ensure Ψ_τ is independent of the sign of fiber directions and in order to predict a stress-free state in the un-deformed configuration, i.e. $\partial\Psi/\partial\mathbf{C} = 0$ when $\mathbf{C} = \mathbf{I}$, as well as the observation of the experimental trends, the angular-base set I_8^* is employed by an exponential-polynomial function as follows to form the interaction potential, i.e.

$$\Psi_\tau = \frac{c_1}{2c_2}\left[\exp\left(c_2\left(I_8^* - \cos(2\theta)\right)^2\right) - 1\right] + c_3\left(I_8^* - \cos(2\theta)\right)^2 \tag{8}$$

where c_1 and c_3 are positive material parameters with the dimension of stress and c_2 is a positive dimensionless parameter. The constant $\cos(2\theta)$ is the cosine of the angle between two line elements in fiber directions at un-deformed configuration. The polynomial term in the right-hand side of the relation (8) enhances greatly the accuracy of the material calibration that is discussed in Section 3. The constitutive behavior of the constituent materials has been well established and is not critical here. So, the isotropic neo-Hookean model (Treloar, 1943) for matrix and the anisotropic model proposed by Holzapfel et al. (2000) are used, i.e.

$$\Psi_\mathrm{F} = \frac{k_1}{2k_2}\sum_{i=4,6}\left[\exp\left(k_2(I_i-1)^2\right) - 1\right], \qquad \Psi_\mathrm{M} = c_{10}(I_1-3) - p(J-1) \tag{9}$$

where k_1 and c_{10} are positive material parameters with the dimension of stress and k_2 is a positive dimensionless material parameter. The scalar p serves as an indeterminate Lagrange multiplier which can be identified as hydrostatic pressure.

Table 1
Material constants of the MFI model.

Contribution	c_{10}, MPa	k_1, MPa	k_2, –	c_1, MPa	c_2, –	c_3, MPa
Matrix	0.380					
Fiber		697.0	1.125e-11			
Interaction				0.0355	9.6790	1.3770

2.4. Cauchy stress

In the following, the decoupled forms $\boldsymbol{\sigma}_I$ and $\boldsymbol{\sigma}_{II}$ of the overall Cauchy stress tensors $\boldsymbol{\sigma}$ corresponding to the potentials (6), (7), and (4), respectively, are presented. A push-forward operation on the second Piola-Kirchhoff stress tensor $\mathbf{S} = 2\partial\Psi(\mathbf{C},\ \{\mathbf{M},\mathbf{N}\})/\partial\mathbf{C}$ with $\mathbf{F}$ results in the Cauchy stress tensor $\boldsymbol{\sigma}$ defined as

$$\boldsymbol{\sigma} = 2\mathbf{F}\frac{\partial\Psi(\mathbf{C},\ \{\mathbf{M},\mathbf{N}\})}{\partial\mathbf{C}}\mathbf{F}^\mathrm{T} = -p\mathbf{I} + 2\frac{\partial\Psi_\mathrm{M}}{\partial I_1}\mathbf{b} + 2\frac{\partial\Psi_\mathrm{F}}{\partial I_4}(\mathbf{m}\otimes\mathbf{m}) + 2\frac{\partial\Psi_\mathrm{F}}{\partial I_6}(\mathbf{n}\otimes\mathbf{n}) + \frac{\partial\Psi_\tau}{\partial I_8^*}\left(\frac{\mathbf{m}\otimes\mathbf{n}+\mathbf{n}\otimes\mathbf{m}}{\sqrt{I_4 I_6}} - I_8^*\left(\frac{\mathbf{m}\otimes\mathbf{m}}{I_4} + \frac{\mathbf{n}\otimes\mathbf{n}}{I_6}\right)\right), \qquad \mathbf{F} = \mathbf{Q}\,\mathbf{f} \tag{10}$$

with $\mathbf{b} = \mathbf{F}\mathbf{F}^\mathrm{T}$, $\mathbf{m} = \mathbf{F}\mathbf{M}$, and $\mathbf{n} = \mathbf{F}\mathbf{N}$ with the components defined as

$$\{\mathbf{m}\} = \{\mathbf{F}\mathbf{M}\} = \begin{bmatrix} m_1 \\ m_2 \\ m_3 \end{bmatrix} = \begin{bmatrix} F_{11}\cos\theta + F_{12}\sin\theta \\ F_{21}\cos\theta + F_{22}\sin\theta \\ 0 \end{bmatrix}, \quad \{\mathbf{n}\} = \{\mathbf{F}\mathbf{N}\} = \begin{bmatrix} n_1 \\ n_2 \\ n_3 \end{bmatrix} = \begin{bmatrix} F_{11}\cos\theta - F_{12}\sin\theta \\ F_{21}\cos\theta - F_{22}\sin\theta \\ 0 \end{bmatrix} \tag{11}$$

The Cauchy stress tensors $\boldsymbol{\sigma}_I$ corresponding to the potential (6) can be determined as

$$\boldsymbol{\sigma}_I = -p\mathbf{I} + 2\frac{\partial\Psi_I}{\partial I_1}\mathbf{b} + \frac{\partial\Psi_I}{\partial I_8^*}\left(\mathbf{m}\otimes\mathbf{n} + \mathbf{n}\otimes\mathbf{m} - I_8^*(\mathbf{m}\otimes\mathbf{m} + \mathbf{n}\otimes\mathbf{n})\right) - \frac{1}{2}q(\mathbf{m}\otimes\mathbf{m}) - \frac{1}{2}r(\mathbf{n}\otimes\mathbf{n}), \quad \mathbf{F}_I = \mathbf{Q}\,\mathbf{f}_\phi^* \tag{12}$$

The indeterminate terms $\mathbf{q} = q(\mathbf{m}\otimes\mathbf{m})$ and $\mathbf{r} = r(\mathbf{n}\otimes\mathbf{n})$ are identified as reaction stresses associated with the fibers inextensibility constraints, with the fiber tensions q and r. The term $1/2\mathbf{q} + 1/2\mathbf{r}$ simplifies the interaction calibration procedure and is not generally considered for computational implementation of the model. The same operation on Ψ_{II} results in

$$\boldsymbol{\sigma}_{II} = -p\mathbf{I} + 2\frac{\partial\Psi_{II}}{\partial I_1}\mathbf{b} + 2\frac{\partial\Psi_{II}}{\partial I_4}(\mathbf{m}\otimes\mathbf{m}) + 2\frac{\partial\Psi_{II}}{\partial I_6}(\mathbf{n}\otimes\mathbf{n}), \quad \mathbf{F}_{II} = \mathbf{Q}\,\mathbf{f}_\mathrm{f}^* \tag{13}$$

3. Constitutive parameter identification

Depending on the chosen coordinate system and complexity of the adopted deformation, the material calibration procedure can become straightforward or difficult. In this work, by adopting simple deformation states the components of the deformation gradient $\mathbf{F}_I$ and $\mathbf{F}_{II}$,

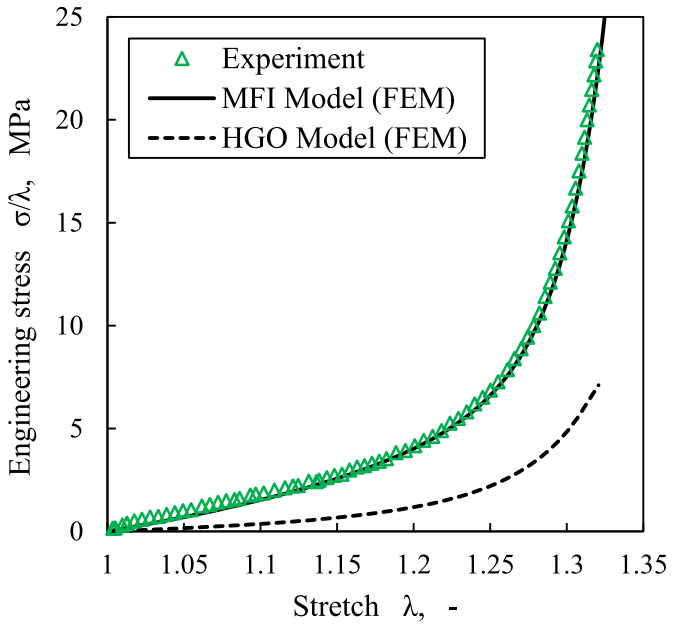

Fig. 2. Comparison of the experimental results of symmetric deformations ($\alpha = -\beta = \pi/4$) with finite element simulation results obtained using the MFI model for the uniaxial extensions in the $\boldsymbol{e}_1$ direction (The material properties provided in Table 1 are used for the simulations). Additionally, the MFI model is compared with the HGO model for the same deformation.

introduced in the previous section, can be easily determined. Upon obtaining their components, the constitutive equations (6) and (7) are rebuilt so as to reconstruct the Cauchy stresses defined in (12) and (13), respectively.

Constituent materials: The material properties of the matrix can be found by performing uniaxial deformation (for more accurate results equi-biaxial tests can be performed optionally) on a pure matrix. For a detailed discussion on the constitutive modeling and experimental characterization of isotropic elastomers, the readers are referred to, for example, Mansouri and Darijani (2014) and Mansouri et al. (2017). Keeping the material parameters of the matrix, unidirectional composites are subjected to uniaxial tests along the fibers direction with a stretch of λ to calibrate the material constants of the fibers potential Ψ_{F}, i.e. k_1 and k_2. The Cauchy stress (13) with its corresponding deformation gradient $\mathbf{F}_{II} = \mathbf{Q}\,\mathbf{f}_{\mathrm{f}}^{*}$ is used. For this specific deformation $\mathbf{Q} = \mathbf{I}$ and the deformation gradient is simplified to $\mathbf{F}_{II} = \mathbf{f}_{\mathrm{f}}^{*} = \mathrm{diag}[\lambda, \lambda^{-1/2}, \lambda^{-1/2}]$. The material properties of the matrix and fibers are given in Table 1.

Mechanical Interactions: Silicone/glass fiber composites with two fiber families, aligned in the $\mathbf{M} = \cos\alpha\,\mathbf{e}_1 + \sin\alpha\mathbf{e}_2$ and $\mathbf{N} = \cos\beta\mathbf{e}_1 + \sin\beta\mathbf{e}_2$ directions with $\alpha = \beta = -\pi/4$, are subjected to uniaxial extensions in the loading direction $\mathbf{e}_1$ to evaluate the interaction properties. The model geometry of the composite strips with a dimension of $\mathrm{a} \times 3l_0$ is shown in the left-hand side of Fig. 1, where $l_0 = \mathrm{a}/\tan\alpha$ and a is the width of the strips. The stress-stretch experimental results of this symmetric deformation are given in Fig. 2. A fixed coordinate system such as $\{\mathbf{e}_1, \mathbf{e}_2, \mathbf{e}_3\}$ is adopted for specifying the loading direction. Bearing in mind that the interaction mechanism is activated due to the rotation of fibers and not of the fibers' elongation, the kinematic constraint I with respective Cauchy stress σ_I defined in (12) is recalled wherein $\mathbf{F}_{\mathrm{I}} = \mathbf{Q}\,\mathbf{f}_{\phi}^{*}$. For this specific deformation $\mathbf{Q} = \mathbf{I}$ and the deformation gradient is given by

$$\mathbf{F}_I = \mathbf{f}_{\phi}^{*} = \begin{bmatrix} \lambda & 0 & 0 \\ 0 & \sqrt{2-\lambda^2} & 0 \\ 0 & 0 & \dfrac{1}{\lambda\sqrt{2-\lambda^2}} \end{bmatrix} \tag{14}$$

where λ is the value of the uniaxial stretch in the loading direction $\mathbf{E}_1$. In order to obtain the unknown scalars of the Cauchy stress (12) with respect to its deformation gradient specified in the above equation, the stress-free boundary conditions are enforced. Using $(\sigma_I)_{33} = 0$ the scalar $p = 2B_{33}\partial\Psi/\partial I_1$ can be determined. The scalars q and r in the Cauchy stress (12) can be also found from $(\sigma_I)_{22} = 0$. Since both families of fibers have the same contributions to the deformation, thus

$$|q| = |\ r| = \frac{2\frac{\partial\Psi_I}{\partial I_1}(b_{22} - b_{33}) + \frac{\partial\Psi_I}{\partial I_8^{*}}\left(2m_2n_2 - I_8^{*}\left(m_2^2 + n_2^2\right)\right)}{m_2^2 + n_2^2} \tag{15}$$

Replacing the values of the scalars p, q, and r in (12), the only non-zero component of the Cauchy stress can be determined as

$$\sigma_I = 2\frac{\partial\Psi_I}{\partial I_1}\left(b_{11} - b_{33} - (b_{22} - b_{33})\frac{m_1^2 + n_1^2}{m_2^2 + n_2^2}\right) + 2\frac{\partial\Psi_I}{\partial I_8^{*}}\left(m_1n_1 - m_2n_2\frac{m_1^2 + n_1^2}{m_2^2 + n_2^2}\right) \tag{16}$$

where $I_1 = \mathrm{tr}(\mathbf{C}_I)$, $I_8^{*} = \mathbf{C}_I : \mathbf{M} \otimes \mathbf{N}$. The values of m_i, n_i, and b_{ij} $i, j\varepsilon\ \{1, 2, 3\}$, are calculated based on the deformation gradient defined in (14). Finally, replacing these values, the Cauchy stress (16) is simplified to

$$\sigma_I = 2\lambda^2\left(\lambda^2 - 1\right)\left(\frac{2\mu}{\lambda^4\left(2 - \lambda^2\right)^2} + c_1\exp\left(c_2\left(\lambda^2 - 1\right)^2\right) + 2c_3\right) \tag{17}$$

This explicit relation for the Cauchy stress in terms of λ, which is reconstructed within the introduced framework, is used for calibration of the mechanical interaction potential to the experimental results. To do this, the Cauchy stress (17), is fitted to the stress-stretch experimental results of the symmetric deformations provided in Fig. 2 using a nonlinear least-squares optimization tool from Matlab. The unknown material constants of the mechanical interaction potential obtained from the calibration procedure are provided in Table 1.

4. Verification of the constitutive behavior

The mechanical interaction potential (Ψ_τ) so calibrated within the

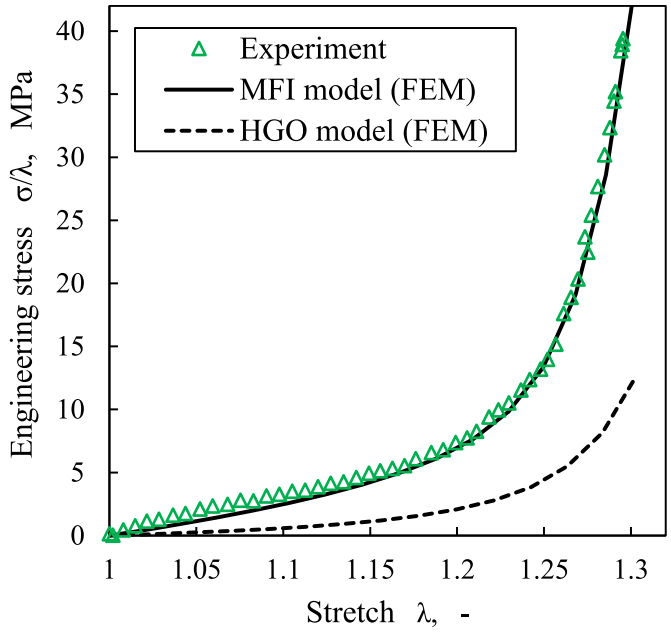

Fig. 3. Comparison of the experimental results of non-symmetric deformations ($\alpha = \pi/6$, $\beta = -\pi/3$) with finite element simulation results obtained using the MFI model for the uniaxial extensions in the $\boldsymbol{e}_1$ direction (The material properties provided in Table 1 are used for the simulations). Additionally, the MFI model is compared with the HGO model for the same deformation.

introduced framework of material characterization (refer to the previous section) and the calibrated constituent potentials (Ψ_M and Ψ_F) are now summed up to form the MFI constitutive model presented in Eq. (4). The MFI model is now verified against two symmetric and non-symmetric deformation states. In doing so, the model is first implemented in the FEM commercial program ABAQUS using a user-defined interface UMAT (the implementation of the model using decoupled forms of the Cauchy stress and elasticity tensors in an Eulerian description is discussed in the upcoming works). The material properties provided in Table 1 are used for the finite element simulations. The geometries are discretized with 3D reduced integration, eight-node linear solid elements with hybrid formulation (C3D8RH). To enforce the incompressibility condition, a large value of the bulk modulus $\kappa = 10^5$ Pa is adopted. The model geometry and the boundary conditions used for the simulations are initially the same as those used in the experiments.

The stress-stretch experimental results provided in Fig. 2 are used as symmetric deformations ($\alpha = \beta = -\pi/4$) for comparison of the model with finite element simulation results. The proposed model is further evaluated in Fig. 3 with comparison to non-symmetric deformation states. In this case, the composites with two fiber families, aligned in the $\mathbf{M} = \cos\alpha\,\mathbf{e}_1 + \sin\alpha\mathbf{e}_2$ and $\mathbf{N} = \cos\beta\mathbf{e}_1 + \sin\beta\mathbf{e}_2$ directions with $\alpha = \pi/6$ and $\beta = -\pi/3$, are subjected to uniaxial extensions in the loading direction $\mathbf{e}_1$. The results respective to both sates of the deformations demonstrate that the predicted responses of the model, so calibrated based on the introduced framework of the material characterization, are in good qualitative agreement with the experimentally observed mechanical behavior of the composites with different material anisotropy.

Note that, the experimental data in Fig. 2 are used for calibration of the mechanical interaction contribution Ψ_τ regardless of the fiber potential Ψ_F through the proposed structurally based framework of the material characterization. The same data are used also for verification of the model against symmetric deformations. These two are different treatments in that the latter is conducted considering both the fibers and the mechanical interaction contributions while the former is done independently of the potential of the fibers. Although the fibers are too stiff, however, they have a considerable contribution to the deformation. That is, both the calibration of the model and its verification through the finite element simulation are independent even though the same experimental data are used for them.

5. The importance of the mechanical interaction potential

There is no any notable declaration on the modifying aspects of including the mechanical interaction potential in overall behavior modeling of the composites until now with exception of a few papers as Guo et al. (2006) and Peng et al. (2013), which are limited to the fitting procedure. As stated, the MFI model along with its structurally based framework of material characterization enables us to obtain distinct contributions of the matrix, fibers, and mechanical interactions. This allows us to highlight the contributions of respective potentials, especially the importance of the mechanical interaction potential, in the modeling of fiber-reinforced elastomers. Toward this end, in the following three representative examples are evaluated: simple uniaxial extension of single layer composites with different material anisotropy, inflation-extension of a cylindrical tube, and load-coupling behaviors in composite laminates with various layups.

5.1. Uniaxial extension of single-layer composites

In the first example, the importance of the mechanical interaction potential Ψ_τ in behavior modeling of composite with different material anisotropy is shown by comparisons of the experimental results with finite element simulations. When the interaction potential is neglected the MFI constitutive model is reduced to the Holzapfel-Gasser-Ogden (HGO) model presented by Holzapfel et al. (2000). Fig. 4 compares

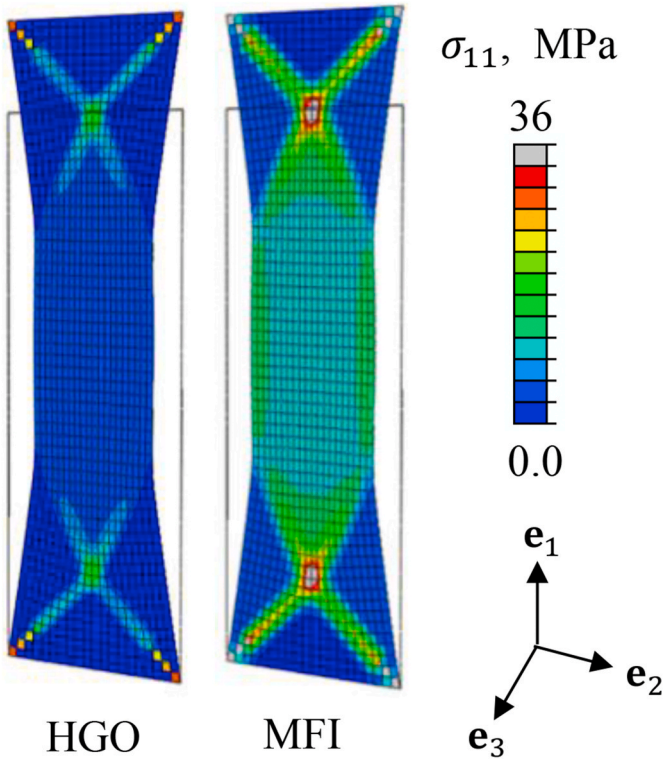

Fig. 4. Spatial distributions of the Cauchy stress σ_{11} using HGO and MFI models for a single layer fiber-reinforced elastomers with two fiber families as $\boldsymbol{M} = \cos\alpha\,\boldsymbol{e}_1 + \sin\alpha\,\boldsymbol{e}_2$ and $\boldsymbol{N} = \cos\beta\,\boldsymbol{e}_1 + \sin\beta\,\boldsymbol{e}_2$ with material anisotropy $\alpha = -\beta = \pi/4$ subjected to a uniaxial stretch of $\lambda_1 = 1.26$ in the $\boldsymbol{e}_1$ direction. The material properties provided in Table 1 are used for simulations

the finite element results of the MFI and HGO models for composites with material anisotropy $\alpha = -\beta = \pi/4$ subjected to the uniaxial extension tests. As it is evident, since the HGO model ignores the mechanical interaction contribution, it underestimates significantly the overall mechanical responses of the composites while the MFI constitutive model predicts the test results accurately. This issue is general and can be extended to all models in which the very important contribution of the mechanical interaction is ignored. In order to show graphically the effect of Ψ_τ for modeling of the latter symmetric deformation, the Cauchy stress distribution σ_{11} corresponding to a stretch of $\lambda_1 = 1.16$ is illustrated in Fig. 4. The geometry and boundary conditions used for simulation is exactly similar to that is used initially by the experiment. The results show a significant difference in the spatial stress distributions made by the incorporation of the interaction potential.

It should be mentioned that the HGO model is originally proposed for modeling the constitutive behavior of biological tissues. However, it is widely used by researchers to model fiber-reinforced inorganic materials, even more so now that it has been implemented in several finite element programs. Accordingly, in this work, the most cited constitutive model of fiber-reinforced elastomers, namely the HGO model, is used for comparative reasons. However, in this work, since the fibers are stiff (recall the material properties of the fibers provided in Table 1, where $k_1 \gg 0$ and $k_2 \approx 0$) an alternative quadratic function with respect to the invariants I_4 and I_6, rather than an exponential function as HGO, can also describe the mechanical behavior of the fibers, i.e.

$$\Psi_F = \frac{k_1}{2}\sum_{i=4,6}(I_i - 1)^2 \tag{18}$$

In the case of non-symmetric deformation states, Fig. 3 compares the finite element results of the MFI and HGO models for composites with material anisotropy $\alpha = \pi/6, \beta = -\pi/3$ subjected to uniaxial extension

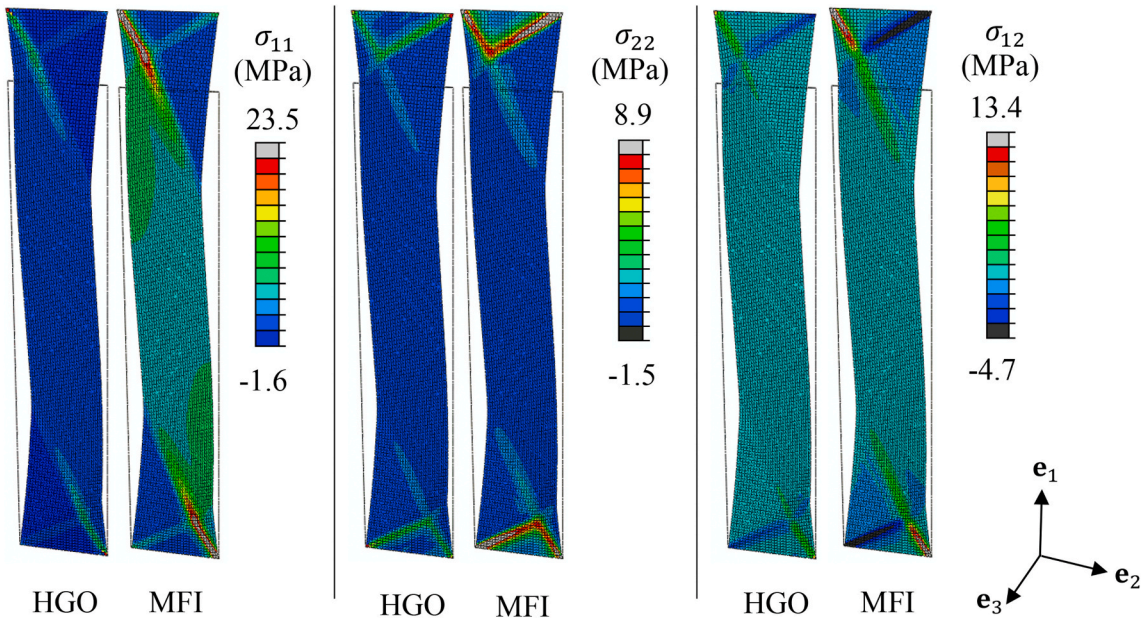

Fig. 5. Finite element simulation of uniaxial extension of a composite with two fiber families as $\boldsymbol{M} = \cos\alpha\, \boldsymbol{e}_1 + \sin\alpha\, \boldsymbol{e}_2$ and $\boldsymbol{N} = \cos\beta\, \boldsymbol{e}_1 + \sin\beta\, \boldsymbol{e}_2$, $\alpha = \pi/6$ and $\beta = -\pi/3$, subjected to a stretch of $\lambda_1 = 1.20$ in the loading direction $\boldsymbol{e}_1$. The effects of the interaction potential Ψ_τ are illustrated by the comparison of the stress distributions obtained from simulation results using the MFI and HGO models, whereas the latter neglects interaction contributions. The material properties provided in Table 1 are used for simulations

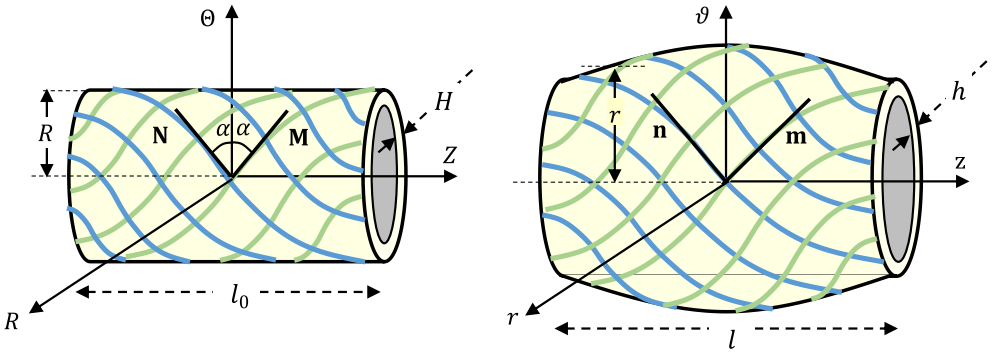

Fig. 6. Section of a long thin-walled cylindrical tube with two fiber families at un-deformed, left, and pressurized configurations, right.

tests explained earlier. As it is evident, again, the HGO model underestimates substantially the mechanical response of the composite while the MFI constitutive model predicts the test results accurately. For further illustrations, respective spatial distributions of the stress components σ_{11}, σ_{12}, and σ_{22} are depicted in Fig. 5 using MFI and HGO models. The same boundary conditions as in the experiment are used for all simulations so that all the nodes of the bottom face of the geometry are constrained and let the top face to be extended freely only in the loading direction $\mathbf{e}_1$ with a stretch of $\lambda_1 = 1.20$ at the top face. The results signify considerable effects of the interaction potential in mechanical behavior modeling of non-symmetric deformation states.

5.2. Inflation-extension of a cylindrical tube

To further illustrate the influence of the mechanical interaction potential in the overall constitutive behavior of fiber-reinforced elastomers, we now consider a complicated deformation as for example inflation-extension of a thin-walled cylindrical tube with closed ends. The cylindrical tubes are popular structures in finite elasticity and are used frequently for evaluation of the mechanical behavior of soft materials under pressure loads (Horný et al., 2015; Masson et al., 2010; Topol et al., 2019; Zidi and Cheref, 2002). The cylindrical tube chosen in this work is subjected to internal pressure P and uniform axial force (due to the internal pressure) at the closed ends of the tube. The two fiber families are initially disposed symmetrically about the circumferential axis Θ with unit vectors $\mathbf{M} = \cos\alpha\, \mathbf{E}_\Theta + \sin\alpha\, \mathbf{E}_Z$ and $\mathbf{N} = \cos\alpha\, \mathbf{E}_\Theta - \sin\alpha\, \mathbf{E}_Z$, $\alpha > 0$, that causes the tube to deform uniformly without twisting, shown in Fig. 6. This figure illustrates a section of a long cylindrical tube with a material point initially located at a Cylindrical basis vector $\{R,\ \Theta,\ Z\}$. During the deformation, this point is mapped into $\{r, \vartheta, z\}$ by a motion with the deformation gradient $\mathbf{F} = \mathrm{diag}[\lambda_r, \lambda_\vartheta, \lambda_z]$, i.e.

$$r = \lambda_\vartheta R, \quad h = \lambda_r H, \quad z = \lambda_z Z, \quad \vartheta = \Theta \tag{19}$$

where λ_z, λ_ϑ and λ_r are principal stretches in axial, circumferential, and radial directions. Here, r and h respectively denote middle radius and thickness with regard to deformed configuration, and H is the initial thickness of the tube. The invariants of the deformation are given by $I_1 = \lambda_r^2 + \lambda_\vartheta^2 + \lambda_z^2$, $I_2 = \lambda_r^{-2} + \lambda_\vartheta^{-2} + \lambda_z^{-2}$, $I_4 = I_6 = \lambda_\vartheta^2 \cos^2\alpha + \lambda_z^2 \sin^2\alpha$ and $I_8 = \lambda_\vartheta^2 \cos^2\alpha - \lambda_z^2 \sin^2\alpha$. For a thin-walled tube, the Cauchy stress in the thickness direction can be considered zero, i.e. $\sigma_{rr} = 0$. Hence, from (10) one obtains the value of the Lagrange multiplier as $p = 2\lambda_r^2 \partial\Psi/\partial I_1$. The circumferential and axial components of the Cauchy stress can be found

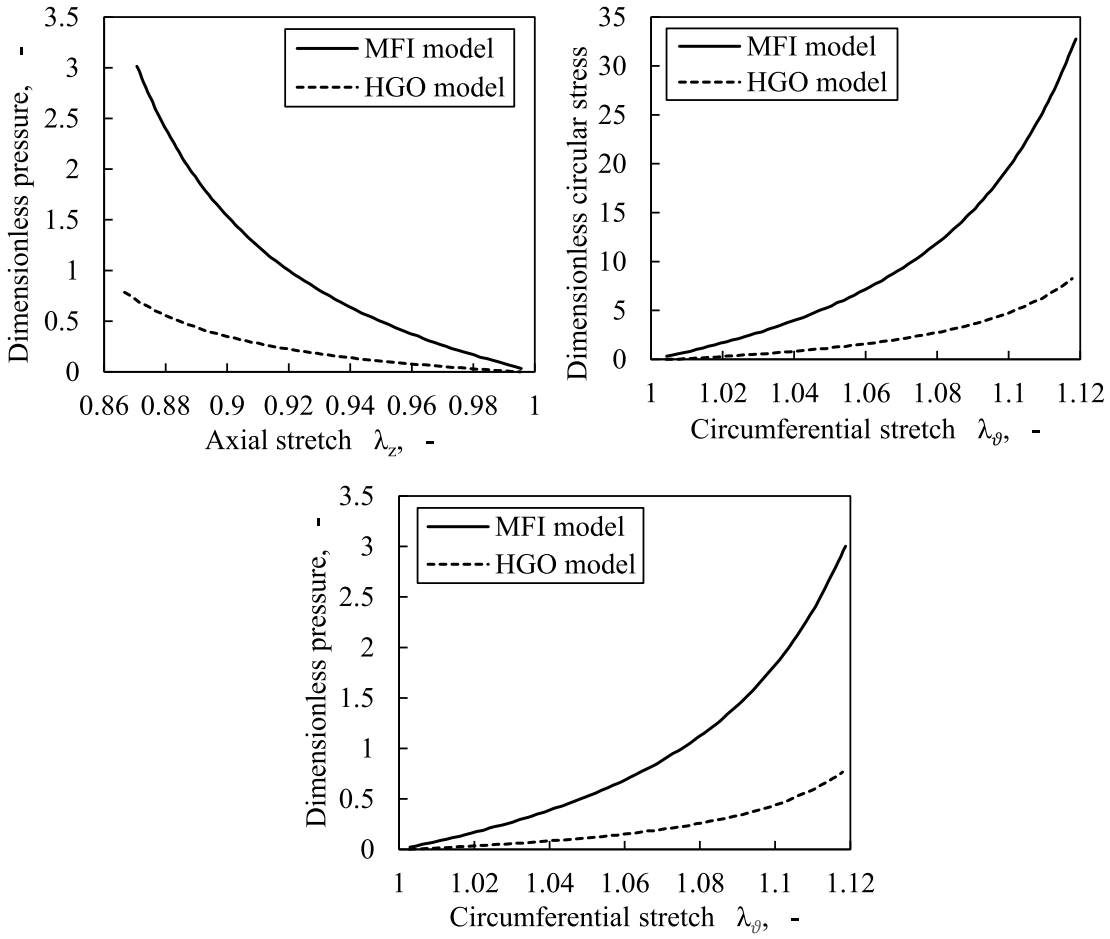

Fig. 7. Inflation-extension responses of a thin-walled cylindrical tube ($\alpha = \pi/4$) using the MFI and HGO models. The weight of the mechanical interaction potential Ψ_τ is featured showing its effects when neglected by comparison of constitutive responses of MFI and HGO models for different quantities. The material properties provided in Table 1 are used for simulations.

by applying equilibrium states of a pressurized tube with internal pressure P as

$$\sigma_{\vartheta\vartheta} = \frac{\mathrm{P}r}{h}, \quad \sigma_{zz} = \frac{\mathrm{P}r}{2h} \qquad \text{or} \qquad \sigma_{\vartheta\vartheta} - 2\sigma_{zz} = 0 \tag{20}$$

Substituting kinematics (19) in (20) gives

$$\sigma_{\vartheta\vartheta} = \frac{\mathrm{P}_d}{\varepsilon}\lambda_\vartheta^2\lambda_z, \quad \sigma_{zz} = \frac{\mathrm{P}_d}{2\varepsilon}\lambda_\vartheta^2\lambda_z \tag{21}$$

with the dimensionless denotations $\varepsilon = H/R$ and $\mathrm{P}_d = P/\ c_{10}$. The circumferential and axial components of the Cauchy stress can be also found from the constitutive equation (10), respectively, as

$$\sigma_{\vartheta\vartheta} = -p + 2c_{10}\lambda_\vartheta^2 + 4\frac{\partial \Psi_{\mathrm{F}}}{\partial I_4}\lambda_\vartheta^2\cos^2\alpha + \frac{2}{I_4}\frac{\partial \Psi_\tau}{\partial I_8^*}\left(1 - I_8^*\right)\lambda_\vartheta^2\cos^2\alpha \tag{22}$$

$$\sigma_{zz} = -p + 2c_{10}\lambda_z^2 + 4\frac{\partial \Psi_{\mathrm{F}}}{\partial I_4}\lambda_z^2\sin^2\alpha - \frac{2}{I_4}\frac{\partial \Psi_\tau}{\partial I_8^*}\left(1 + I_8^*\right)\lambda_z^2\sin^2\alpha \tag{23}$$

Note that herein, the deformation is homogeneous and hence the shear components of the stress are zero. From the incompressibility condition, one obtains $\lambda_r = \lambda_\vartheta^{-1}\lambda_z^{-1}$. Substituting the values of p and λ_r in (22) and (23) gives $\sigma_{\vartheta\vartheta}$ and σ_{zz} as functions of both circumferential and axial stretches. To find numerically a relation between the stretches λ_ϑ and λ_z the equilibrium function defined in Eq. $(20)_2$ is solved by minimizing the objective function of $\langle \sigma_{\vartheta\vartheta} - 2\sigma_{zz}\rangle^2$. It is done for unknown λ_z with prescribed values of λ_ϑ. Next, combining equations (21)–(23), one obtains relations that govern inflation load (P_d) to circumferential and axial directions (λ_ϑ, λ_z). Inflation-extension behavior of the thin-walled cylindrical tube considering the MFI and HGO constitutive models is plotted in Fig. 7 using the material properties provided in Table 1 and considering $\varepsilon = 0.1$. In view of these results, one can claim the substantial weight of the mechanical interaction potential for behavior modeling of the pressurized thin-walled cylindrical tubes.

5.3. Load-coupling behaviors

The primary purpose of the mechanical characterization of the single-layer composites is designing composite laminates aiming at pronounced functionalities. Load coupling effects, e.g. extension-twist coupling, are among interesting functionalities offering a huge potential for completely new application concepts such as the field of elastofluidics (Bishop-Moser, 2014; Felt et al., 2017; Felt and Remy, 2018). In this section, the importance of mechanical interaction potential is evaluated for modeling the load-coupling behaviors in fiber-reinforced composite laminates. To do this, a composite laminate with two layers and material anisotropy as $[+\ 45\ -\ 45/+\ 30-\ 60]$ is subjected to a uniaxial displacement of $d = 5$ mm in the loading direction $\mathbf{e}_1$ applied on the front face as shown in Fig. 8. The material anisotropy of each layer is disposed about the direction $\mathbf{e}_1$. Each layer has the same model geometry with the dimension of $100 \times 50 \times 2$ (mm $\times$mm $\times$mm) aligned with the axes $\mathbf{e}_1$, $\mathbf{e}_2$, and $\mathbf{e}_3$. All nodes of the front and back face of the geometry are fixed with the exception that the nodes of the front face are allowed to elongate and rotate along and about $\mathbf{e}_1$, respectively. During the extension of the composite, load coupling effects in the form of

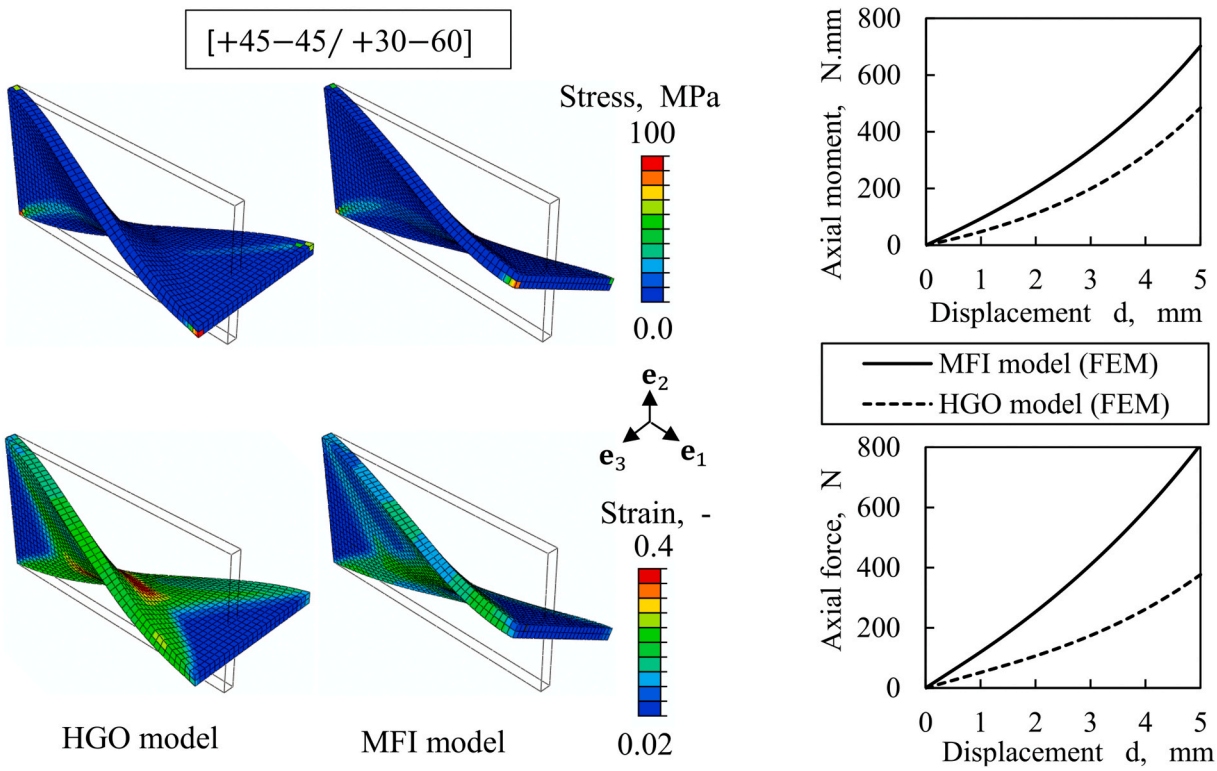

Fig. 8. The effect of the mechanical interaction potential in load-coupling behavior modeling of a composite laminate using the MFI and HGO constitutive models for a displacement of $d = 5$ mm in the loading direction e_1. Moment-displacement and force-displacement responses are also compared.

extension-twist deformations are observed in Fig. 8. In this figure, the load-coupling behaviors are modeled using the MFI and HGO constitutive models and the corresponding spatial distributions of the stresses and strains are shown there. The results indicate that not only significant differences are observed in the stresses and strains distributions but also the mechanical interaction contribution highly affects the amount of twisting, which results in different final configurations. For a quantitative evaluation of the interaction potential, the force-displacement and moment-displacement responses of the same laminate are provided in this figure.

6. Conclusions

A unified invariant-base constitutive model for hyperelastic fiber-reinforced elastomers with two fiber families considering the contributions of the matrix, fiber, and particularly the mechanical interactions, so-called the MFI model, is proposed. An extensional-base invariant set is used by the fibers' potential and an angular-base invariant is employed by an exponential-polynomial function to form the mechanical interaction potential. In an effort to find the mechanical interaction properties regardless of the fibers potential, a workless reaction term consistent with the kinematics of the mechanical interactions is added to the mechanical interaction potential. The above-mentioned adoptions introduce a structurally based framework for material characterization of such composites. The following features can be stated for the MFI model characterized within the introduced framework of material characterization:

- Experimental advantage. The anisotropy can be characterized completely with the least number of required tests using simple uniaxial extension tests rather than complicated ones such as biaxial deformations.
- Accuracy. The proposed model enables us to capture the mechanical behavior of fiber-reinforced elastomers with two fiber families and with different material anisotropy (see the previous section). It is shown by the comparison of experiments with finite element simulations for symmetric and non-symmetric deformation states.
- Utility. The mechanical interaction properties are obtained within the introduced framework by fitting the Cauchy stress (17) to the stress-stretch response of the symmetric deformations featured in Section 4.

In order to show the importance of the mechanical interactions in constitutive modeling of fiber-reinforced elastomers, three representative examples are provided: uniaxial extension of single-layer composites with different material anisotropy, inflation-extension of a thin-walled cylindrical tube, and extension-twist coupling behaviors in composite laminates subjected to uniaxial extensions are all modeled using the MFI and HGO constitutive models. The results imply that the mechanical interaction potential affects substantially the constitutive behavior of the fiber-reinforced elastomers. This work contributes to the importance of the mechanical interaction for modeling of inorganic materials, yet remains to wait for biomaterials, particularly since recently Holzapfel and Ogden (2019) proposed a model accounting for coupling between the collagen fiber and cross-link directions in arterial walls.

CRediT authorship contribution statement

M.R. Mansouri: Conceptualization, Software, Investigation, Formal analysis, Writing - original draft. **P.F. Fuchs:** Funding acquisition, Supervision, Writing - review & editing. **J.C. Criscione:** Writing - review & editing. **B. Schrittesser:** Supervision, Writing - review & editing. **J. Beter:** Investigation.

Declaration of competing interest

The authors declare that they have no known competing financial

interests or personal relationships that could have appeared to influence the work reported in this paper.

Acknowledgement

The research work was performed at the Polymer Competence Center Leoben GmbH (PCCL, Austria) within the framework of the COMET-program of the Federal Ministry of Science, Research and Economy with contributions by Montanuniversitaet Leoben (Chair of Materials Science and Testing of Polymers, Austria).

Appendix A

The free energy of fiber-reinforced elastomers must be unchanged if a deformed configuration by $\mathbf{f}$ occupying a region as $\overline{\mathbf{\Omega}}$ undergoes a rotation described by the proper orthogonal tensor $\mathbf{Q}$ such that $\mathbf{Q}^{\mathrm{T}}\mathbf{Q} = \mathbf{I}$ and $\det\mathbf{Q} = 1$. The deformed region $\overline{\mathbf{\Omega}}$ relative to the deformation gradient $\mathbf{f}$ is rotated to the final configuration B, i.e.

$$\mathbf{F} = \mathbf{Q}\,\mathbf{f} \tag{A.1}$$

Since $\mathbf{C} = \mathbf{F}^{\mathrm{T}}\mathbf{F} = \mathbf{f}^{\mathrm{T}}\mathbf{f} = \mathbf{U}^2$, the deformation gradients $\mathbf{F}$ and $\mathbf{f}$ share the same Lagrangian strain.

Criscione and Hunter (2003) proposed three strain attributes in the basis of three scalars $\{\alpha_c,\ \mathscr{B},\ \gamma\}$ for *thin incompressible* fiber-reinforced elastomers with two fiber families (For a detailed discussion, the authors are referred to the referenced paper). The scalar α_c is area ratio of the fiber plane $(\mathbf{E}_1 - \mathbf{E}_2)$ due to distortion keeping the fibers angle without change, $\mathscr{B}$ represents the change of the angle between fibers of the same stretch, and γ is a shear strain in the fiber plane that differentially changes the length of deformed elements yet does not perturb the angle. They introduced the following relations between the strain attributes and invariants of the deformation described earlier as

$$\sqrt{I_4 I_6} = \alpha_c\left(\mathscr{B}^2 c^2 + \mathscr{B}^{-2} s^2\right) \tag{A.2}$$

$$\frac{\sqrt{I_4}}{\sqrt{I_6}} = \frac{\sqrt{1+\gamma^2 s^2 c^2} - \gamma sc}{\sqrt{1+\gamma^2 s^2 c^2} + \gamma sc} \tag{A.3}$$

wherein $c = \cos\theta$ and $s = \sin\theta$. They factored $\mathbf{f}$ into modes of deformation corresponding to the three scalar strain attributes as follows:

$$\mathbf{f} = \mathbf{f}_{\alpha_c}\mathbf{f}_{\mathscr{B}}\mathbf{f}_{\gamma} \tag{A.4}$$

Upon setting the kinematics constraint I (recall Eq. (4)), i.e. $I_4 = I_6 = 1$, in Eqs. (A.2) and (A.3), and considering the relation $(3)_2$, it is straightforward to show, respectively, that

$$\alpha_c = \left(\mathscr{B}^2 c^2 + \mathscr{B}^{-2} s^2\right)^{-1},\ \gamma = 0,\ \mathscr{B} = g(\phi) \tag{A.5}$$

where g shows a functional dependency of β to the current angle ϕ. The three relations in (A.5) show that, under constraint I, all the deformation scalars $\{\alpha_c,\ \mathscr{B},\ \gamma\}$ are reduced to $\{\mathscr{B}\}$ and therefore, from $\mathscr{B} = g(\phi)$, depend on ϕ. Now upon replacing the scalars of (A.5) in (A.4) it is found that the components of $\mathbf{f}$ can be given in terms of ϕ, i.e. $\mathbf{f} = \mathbf{f}^*_{\phi}$. Accordingly, under constraint I, the *entire* deformation field given by (A.1) is then defined specifically in terms of the change of the angle between fibers through $\mathbf{f}^*_{\phi}$ super-imposed by a rigid-body motion, $\mathbf{Q}$, i.e.

$$\mathbf{F}_I = \mathbf{Q}\,\mathbf{f}^*_{\phi} \tag{A.6}$$

The second kinematic constraint defined in Eq. (4) represents the case where the current angle between fibers, ϕ, is held constant while the elongation of the fibers is allowed. Hence, replacing the constraint $\phi = 2\theta$ in $(3)_2$ yields

$$\cos 2\,\theta = \frac{1-\tan^2\theta}{1+\tan^2\theta} = \frac{\mathscr{B}^2\cos^2\theta - \mathscr{B}^{-2}\sin^2\theta}{\mathscr{B}^2\cos^2\theta + \mathscr{B}^{-2}\sin^2\theta} \tag{A.7}$$

Upon doing some algebra on the right-hand side of the equation, it is found that $\mathscr{B} = 1$. With substitution into (A.2) and considering the equation (A.3), the three scalars can be written as

$$\alpha_c = \sqrt{I_4 I_6}\ ,\qquad \mathscr{B} = 1,\qquad \gamma = h(I_4, I_6) \tag{A.8}$$

where $\gamma = h(I_4, I_6)$ shows functional dependency of γ to the extensional-base invariants I_4 and I_6. Bearing in mind that γ differentially changes the length of deformed elements yet does not perturb the angle and replacing the scalars defined in (A.8) into relation (A.4) it yields $\mathbf{f} = \mathbf{f}^*_{\mathrm{f}}$, where the components of $\mathbf{f}^*_{\mathrm{f}}$ have a functional dependency on the extensional-base invariants I_4 and I_6. For this case, the deformation gradient (A.1) is therefore defined as

$$\mathbf{F}_{II} = \mathbf{Q}\,\mathbf{f}^*_{\mathrm{f}} \tag{A.9}$$

References

Alhayani, A.A., Rodríguez, J., Merodio, J., 2014. Competition between radial expansion and axial propagation in bulging of inflated cylinders with application to aneurysms propagation in arterial wall tissue. Int. J. Eng. Sci. 85, 74–89.

Bishop-Moser, J.L., 2014. Design of Generalized Fiber-Reinforced Elasto-Fluidic Systems.

Chaimoon, K., Chindaprasirt, P., 2019. An anisotropic hyperelastic model with an application to soft tissues. Eur. J. Mech. Solid. 78, 103845.

Chebbi, E., Wali, M., Dammak, F., 2016. An anisotropic hyperelastic constitutive model for short glass fiber-reinforced polyamide. Int. J. Eng. Sci. 106, 262–272.

Connolly, F., Wagner, D.A., Walsh, C.J., Bertoldi, K., 2019. Sew-free anisotropic textile composites for rapid design and manufacturing of soft wearable robots. Extreme Mechan. Lett. 27, 52–58.

Criscione, J.C., Hunter, W.C., 2003. Kinematics and elasticity framework for materials with two fiber families. Continuum Mech. Therm. 15 (6), 613–628.

Felt, W., Remy, C.D., 2018. A closed-form kinematic model for fiber-reinforced elastomeric enclosures. J. Mech. Robot. 10 (1), 14501.

Felt, W., Telleria, M.J., Allen, T.F., Hein, G., Pompa, J.B., Albert, K., Remy, C.D., 2017. An inductance-based sensing system for bellows-driven continuum joints in soft robots. Aut. Robots 1–14.

Fereidoonnezhad, B., Naghdabadi, R., Arghavani, J., 2013. A hyperelastic constitutive model for fiber-reinforced rubber-like materials. Int. J. Eng. Sci. 71, 36–44.

Gong, Y., Peng, X., Yao, Y., Guo, Z., 2016. An anisotropic hyperelastic constitutive model for thermoplastic woven composite prepregs. Compos. Sci. Technol. 128, 17–24.

Gong, Y., Yan, D., Yao, Y., Wei, R., Hu, H., Xu, P., Peng, X., 2017. An anisotropic hyperelastic constitutive model with tension–shear coupling for woven composite reinforcements. Int. J. Appl. Mech. 9 (6), 1750083.

Guo, Z.Y., Peng, X.Q., Moran, B., 2006. A composites-based hyperelastic constitutive model for soft tissue with application to the human annulus fibrosus. J. Mech. Phys. Solid. 54 (9), 1952–1971.

Holzapfel, G.A., Gasser, T.C., 2001. A viscoelastic model for fiber-reinforced composites at finite strains: continuum basis, computational aspects and applications. Comput. Methods Appl. Mech. Eng. 190 (34), 4379–4403.

Holzapfel, G.A., Gasser, T.C., Ogden, R.W., 2000. A new constitutive framework for arterial wall mechanics and a comparative study of material models. J. Elasticity Phys. Sci. solids 61 (1), 1–48. https://doi.org/10.1023/A:1010835316564.

Holzapfel, G.A., Ogden, R.W., 2009. Constitutive modelling of passive myocardium: a structurally based framework for material characterization. Phil. Trans. Roy. Soc. Lond.: Math. Phys. Eng. Sci. 367 (1902), 3445–3475.

Holzapfel, G.A., Ogden, R.W., 2019. An arterial constitutive model accounting for collagen content and cross-linking. J. Mech. Phys. Solid. 103682.

Horný, L., Netušil, M., Horák, Z., 2015. Limit point instability in pressurization of anisotropic finitely extensible hyperelastic thin-walled tube. Int. J. Non Lin. Mech. 77, 107–114.

Liu, H., Holzapfel, G.A., Skallerud, B.H., Prot, V., 2019. Anisotropic finite strain viscoelasticity: constitutive modeling and finite element implementation. J. Mech. Phys. Solid. 124, 172–188.

Mansouri, M.R., Darijani, H., 2014. Constitutive modeling of isotropic hyperelastic materials in an exponential framework using a self-contained approach. Int. J. Solid Struct. 51 (25), 4316–4326. https://doi.org/10.1016/j.ijsolstr.2014.08.018.

Mansouri, M.R., Darijani, H., Baghani, M., 2017. On the correlation of FEM and experiments for hyperelastic elastomers. Exp. Mech. 57 (2), 195–206. https://doi.org/10.1007/s11340-016-0236-0.

Masson, I., Fassot, C., Zidi, M., 2010. Finite dynamic deformations of a hyperelastic, anisotropic, incompressible and prestressed tube. Applications to in vivo arteries. Eur. J. Mech. Solid. 29 (4), 523–529.

Melnik, A.V., Luo, X., Ogden, R.W., 2018. A generalised structure tensor model for the mixed invariant I8. Int. J. Non Lin. Mech. https://doi.org/10.1016/j.ijnonlinmec.2018.08.018.

Merodio, J., Saccomandi, G., 2006. Remarks on cavity formation in fiber-reinforced incompressible non-linearly elastic solids. Comput. Mater. Sci. 25 (5), 778–792.

Milani, A.S., Nemes, J.A., 2004. An intelligent inverse method for characterization of textile reinforced thermoplastic composites using a hyperelastic constitutive model. Compos. Sci. Technol. 64 (10–11), 1565–1576.

Murphy, J.G., 2013. Transversely isotropic biological, soft tissue must be modelled using both anisotropic invariants. Eur. J. Mech. Solid. 42, 90–96.

Peng, X., Guo, G., Zhao, N., 2013. An anisotropic hyperelastic constitutive model with shear interaction for cord–rubber composites. Compos. Sci. Technol. 78, 69–74.

Peng, X.Q., Guo, Z.Y., Moran, B., 2006. An anisotropic hyperelastic constitutive model with fiber-matrix shear interaction for the human annulus fibrosus. J. Appl. Mech. 73 (5), 815–824.

Ren, J.-s., Zhou, J.-w., Yuan, X., 2011. Instability analysis in pressurized three-layered fiber-reinforced anisotropic rubber tubes in torsion. Int. J. Eng. Sci. 49 (4), 342–353.

Spencer, A.J.M., 1984. Constitutive theory for strongly anisotropic solids. In: Continuum Theory of the Mechanics of Fibre-Reinforced Composites. Springer, pp. 1–32.

Topol, H., Demirkoparan, H., Pence, T.J., 2019. Morphoelastic fiber remodeling in pressurized thick-walled cylinders with application to soft tissue collagenous tubes. Eur. J. Mech. Solid. 77, 103800.

Treloar, L.R.G., 1943. The elasticity of a network of long-chain molecules. I. Trans. Faraday Soc. 39, 36–41.

Tricerri, P., Dedè, L., Gambaruto, A., Quarteroni, A., Sequeira, A., 2016. A numerical study of isotropic and anisotropic constitutive models with relevance to healthy and unhealthy cerebral arterial tissues. Int. J. Eng. Sci. 101, 126–155.

Wagner, D.R., Lotz, J.C., 2004. Theoretical model and experimental results for the nonlinear elastic behavior of human annulus fibrosus. J. Orthop. Res. 22 (4), 901–909.

Zidi, M., Cheref, M., 2002. Finite deformations of a hyperelastic, compressible and fibre reinforced tube. Eur. J. Mech. Solid. 21 (6), 971–980.